JGR Space Physics

RESEARCH ARTICLE
10.1029/2026JA035058

Key Points:
- Two-dimensional simulations are performed to study the compressive structures formed during ion-ion beam instabilities
- Quasi-parallel waves are initially excited by ion-ion beam instabilities, and their amplitudes saturate in later stages
- When the beam plasma temperature is sufficiently high, quasi-perpendicular modes grow to form compressive structures

Correspondence to:
Q. Lu and X. Gao,
qmlu@ustc.edu.cn;
gaoxl@ustc.edu.cn

Citation:
Ren, J., Lu, Q., Gao, X., Guo, J., Lu, S., & Wang, R. (2026). Two-dimensional hybrid simulations of compressive structures formed during ion-ion beam instabilities. *Journal of Geophysical Research: Space Physics*, *131*, e2026JA035058. https://doi.org/10.1029/2026JA035058

Received 8 JAN 2026
Accepted 7 JUN 2026

Two-Dimensional Hybrid Simulations of Compressive Structures Formed During Ion-Ion Beam Instabilities

Junyi Ren[1], Quanming Lu[1,2], Xinliang Gao[1,2], Jin Guo[1], San Lu[1,2], and Rongsheng Wang[1,2]

[1]Deep Space Exploration Laboratory, School of Earth and Space Sciences, University of Science and Technology of China, Hefei, China, [2]Collaborative Innovation Center of Astronautical Science and Technology, Harbin, China

Abstract Foreshock compressive structures are often linked to the formation of magnetosheath jets—high dynamic pressure structures frequently observed downstream of quasi-parallel shocks. Formation of these structures is attributed to the nonlinear evolution of foreshock waves excited by ion-ion beam instabilities. However, the conditions and underlying mechanisms forming these compressive structures remain unclear. In this study, we investigate the evolution of ion-ion beam instabilities using two-dimensional hybrid simulations with the continuous injection of ion beams. Our results demonstrate that while quasi-parallel waves are initially excited, quasi-perpendicular, compressive, non-propagating modes—likely formed by nonlinear wave superposition—grow to large amplitudes when the beam ion temperature is sufficiently high, eventually evolving into compressive structures. In contrast, these quasi-perpendicular modes saturate at small amplitudes, and no significant compressive structures form when the beam ion temperature is insufficient.

1. Introduction

The structure and dynamics of collisionless shocks and the downstream magnetosheaths are fundamentally governed by the orientation of the interplanetary magnetic field (Burgess, 1989; Leroy et al., 1982; Tang et al., 2025). At a quasi-parallel shock, where the angle between the shock normal and the upstream magnetic field is less than 45°, the shock front and downstream magnetosheath are turbulent. A prominent feature observed downstream of such shocks is the presence of magnetosheath jets—localized enhancements of dynamic pressure (Hietala et al., 2009; Němeček et al., 1998; Plaschke et al., 2013). Magnetosheath jets are frequently observed downstream of planetary bow shocks (Gunell et al., 2023; Guo et al., 2024; Karlsson et al., 2016; Plaschke et al., 2016; Zhou et al., 2024) and interplanetary shocks (Hietala et al., 2024), and their occurrence is prominent in the subsolar region behind the Earth's bow shock (Archer & Horbury, 2013; Guo et al., 2022; Plaschke et al., 2013). These structures typically exhibit enhanced plasma density and velocity, alongside temperatures lower than the surrounding plasma (Archer & Horbury, 2013; Fatemi et al., 2024). The magnetosheath jets can be geo-effective; large-scale jets can impinge upon and distort the magnetopause (Archer et al., 2019; Guo et al., 2026; Němeček et al., 2023; Plaschke et al., 2016; Ren et al., 2024; Yang et al., 2024), potentially triggering complex responses in the magnetosphere and ionosphere (Han et al., 2016; Ma et al., 2024; Wang et al., 2018). The origin of these structures is inextricably linked to kinetic processes in the upstream region. These include processes associated with solar wind discontinuities (Archer et al., 2012; Dmitriev & Suvorova, 2012; Lin et al., 1996; Zhou et al., 2024) and foreshock waves under quiet solar wind conditions (Hietala et al., 2009; Omidi et al., 2013; Raptis et al., 2022), particularly the compressive structures formed during wave evolution (Palmroth et al., 2018; Ren et al., 2023; Suni et al., 2021).

At quasi-parallel shocks, a fraction of incident solar wind ions is reflected at the shock front, streaming back upstream to form ion beams (Gosling et al., 1989; Hao et al., 2016). These beams provide the free energy necessary to drive three primary types of ion-ion beam instabilities. When the beam velocity is sufficiently high, the system becomes susceptible to the right-hand resonant instability, which excites a quasi-parallel, right-hand polarized magnetosonic mode wave (Hoppe & Russell, 1983; Gary, 1991; Lu et al., 2006). The maximum growth rate of the right-hand resonant instability is primarily governed by the beam density (Gary, 1978). Conversely, when the beam temperature is sufficiently high such that the thermal speed of the beam ions exceeds their drift velocity, Alfvén mode waves can be excited via the left-hand resonant instability (Eastwood et al., 2003; Gary, 1985). Alternatively, a cold, fast beam can trigger the non-resonant instability, exciting right-hand waves that propagate against the beam (Burgess & Scholer, 2015). Although waves excited by all three instabilities have been observed in the Earth's foreshock, the right-hand resonant wave, typically exhibiting a period of approximately 30 s ("30-s waves"), is the most ubiquitous (Fairfield, 1969; Narita et al., 2006).

As these waves propagate and are convected toward the shock front, the velocity distribution of the beam ions is continually modified by the waves they generate. In the vicinity of the quasi-parallel shock front, the shock-reflected ions are thermalized into a "diffuse" distribution, characterized by a flat energy spectrum and a broad angular distribution (Bonifazi & Moreno, 1981). In regions further upstream, however, the beam ions tend to exhibit a lower temperature (Kempf et al., 2015). When the waves encounter the diffuse ion population as they are brought back to the shock front by the solar wind, they steepen to form shocklets or short, large-amplitude magnetic structures (SLAMS) (Schwartz & Burgess, 1991; Scholer et al., 2003; Tsubouchi & Lembège, 2004). Consequently, the wave normal is deflected to align parallel with the shock normal (Dubouloz & Scholer, 1995; Scholer et al., 1993). These structures trap the thermalized diffuse ions in the vicinity of the shock front (Su et al., 2012) and can steepen to an amplitude exceeding that of the shock front itself, thereby completing cyclic shock reformation processes (Hao et al., 2017; Tsubouchi & Lembège, 2004).

The waves excited by the three primary instabilities all propagate either quasi-parallel or anti-parallel to the beam direction. However, the structures relevant to large-scale magnetosheath jets possess a normal direction perpendicular to the background magnetic field (Ren et al., 2023), requiring the excitation of a perpendicular wave mode. Several candidate mechanisms have been proposed to explain their formation. First, linear theory predicts a positive growth rate for a highly oblique wave mode if the beam is sufficiently dense (Hellinger & Mangeney, 1999). Furthermore, wave-particle interactions in the foreshock region scatter the beam ions into partial-shell or ring-beam distributions (Kempf et al., 2015), which are also unstable to oblique perturbations (Blanco-Cano et al., 2009; Hao et al., 2021). Second, perpendicular fluctuations can be generated through nonlinear processes. Two quasi-parallel modes can superpose to form a second-order mode whose wave number and frequency correspond to the differences of the first-order modes (Vasquez & Hollweg, 1999). When the two quasi-parallel modes possess identical parallel wave numbers and frequencies, a perpendicular, pressure-balancing mode is generated. This mode is observed as filamentary structures in simulations of ion-ion beam instabilities (Wang & Lin, 2003, 2006). A third mechanism leading to perpendicular inhomogeneity involves feedback from the shock front. Quasi-parallel shocks intrinsically possess rippled shock fronts (Gingell et al., 2017; Scholer et al., 1993). Ions are reflected differently across various parts of a rippled shock front: specifically, ions are less likely to be reflected where the shock front dents downstream (Hao et al., 2016). Because these ions travel along the magnetic field lines, the spatial differences in ion reflection can potentially generate perpendicular foreshock inhomogeneities.

This study explores the conditions necessary for the formation of these jet-related, perpendicular compressive structures. Specifically, we investigate whether these structures arise from a feedback loop between the shock front and the foreshock, or if they are intrinsic to ion-ion beam unstable systems and thus dependent on beam properties. To achieve this, we perform two-dimensional (2D) hybrid simulations with a continuously injected ion beam to investigate the nonlinear evolution of ion-ion beam instabilities. By varying the temperature of the injected ion beam, we elucidate the conditions and mechanisms governing the formation of compressive foreshock structures, providing insight into the genesis of magnetosheath jets.

2. Simulation Setups

In this study, we employ the Hybrid-VPIC code (Le et al., 2023) with a continuous beam injection setup to investigate the formation of compressive structures driven by ion-ion beam instabilities. The simulation domain comprises $n_x \times n_y = 1008 \times 512$ grid cells with a spatial resolution of $\Delta x = \Delta y = 1\ d_i$ (ion inertial length) and a temporal resolution of $\Delta t = 0.01\ \Omega_i^{-1}$ (inverse ion gyro-frequency). The system is initialized with a uniform magnetic field, B_0, parallel to the x-axis, which is the favored condition for the formation of large-scale magnetosheath jets (Guo et al., 2022; Ren et al., 2023). The background "solar wind" ions are initialized uniformly with density N_0, plasma $\beta = 1$, and a bulk velocity $\mathbf{V}_0 = (-7, 0, 0)\ V_{A0}$, where $V_{A0} = B_0/\sqrt{\mu_0 m_i N_0}$ denotes the Alfvén speed. The simulation domain employs periodic boundaries in the y-direction.

Table 1
Temperature of the Injected Ion Beams

Case	1	2	3	4
$T_b/(m_i V_{A0}^2)$	1	10	20	50

The boundary conditions along the x-axis, which is parallel to the background magnetic field, require careful consideration. Previous simulations of ion-ion beam instabilities often employed periodic boundary conditions in the x-direction, initializing the system with core and beam ion components (Hellinger & Mangeney, 1999; Wang & Lin, 2003). However, in these models, the resulting compressive structures either exhibit substantially lower amplitudes than the parallel waves (Wang & Lin, 2003; Wang & Lin, 2006) or dissipate entirely during the late stages of the simulation (Hellinger & Mangeney, 1999). This indicates that a periodic boundary setup fails to capture the essential physics required to generate large-amplitude compressive structures. A primary distinction between this classical setup and the realistic foreshock environment is that, in the latter, waves continuously encounter fresh, dense beam populations as they are convected toward the shock by the upstream flow. Therefore, the simulation setup must provide a sustained supply of beam ions to interact with the excited waves.

Another widely utilized approach implements a reflecting wall at one of the x-boundaries, allowing a shock to form and reflect ions self-consistently (Hao et al., 2021; Ren et al., 2023). However, this configuration precludes us from distinguishing whether the compressive structures are intrinsic to systems unstable to ion-ion beam instabilities or if they originate from a feedback loop built upon inhomogeneous shock reflections (Hao et al., 2016). Consequently, the shock front must be excluded from the simulation domain.

Our simulation resolves these problems by applying open/absorbing conditions to both of the x-boundaries. The background ions and beam ions are continuously injected from the $+x$ and $-x$ boundaries, respectively. The background ions are injected with a speed of $\mathbf{V}_0$, which is sufficiently high to prevent a shock from forming within the simulation domain. The beam ions injected from the $-x$ boundary have a density $N_b = 0.02\ N_0$ and bulk velocity $\mathbf{V}_b' = (3,0,0)\ V_{A0}$, resulting in a total beam speed of $V_b = |\mathbf{V}_b - \mathbf{V}_0| = 10\ V_{A0}$. The solar wind and beam parameters are chosen according to typical values reported in observations (Bonifazi & Moreno, 1981) and simulations (Kempf et al., 2015). There are 150 macro particles on average initialized per grid cell in the simulation domain for the background ions, and the beam ions are injected with an equivalent number density flux. The critical parameter in this study is the temperature of the beam ions, T_b. We conduct four simulations (Cases 1–4) with varying T_b, as detailed in Table 1.

3. Simulation Results

We first focus on the temporal evolution of the amplitude of the excited waves. To separate the transverse and the compressive components, we define the compressive ($\delta B_{\parallel}$) and transverse ($\delta B_{\perp}$) wave amplitudes as the root-mean-square of the magnetic field fluctuations integrated over the relevant wavenumbers:

$$\delta B_{\parallel} = \sqrt{\sum_k |\delta B_x|^2}, \quad \delta B_{\perp} = \sqrt{\sum_k |\delta B_y|^2 + \sum_k |\delta B_z|^2}, \tag{1}$$

and the total fluctuation is calculated by $\delta B = \sqrt{\delta B_{\parallel}^2 + \delta B_{\perp}^2}$. The integration domains are defined as $0 \le k_x < 0.03, |k_y| < 0.2$ for the compressive fluctuations and $0.04 \le k_x < 0.2, |k_y| < 0.2$ for the transverse fluctuations; most of the wave power of interest is concentrated in these regions, as will be shown in Figures 4 and 6. Figure 1 shows the temporal evolution of the transverse and compressive amplitudes, as well as the ratio of the compressive to the total amplitude. The evolution of the waves proceeds in three distinct stages. In the initial phase ($t \lesssim 150\ \Omega_i^{-1}$), the waves exhibit quasi-linear growth with simultaneous amplification of both transverse and compressive components. Subsequently, the wave-particle interactions lead to the saturation of the transverse component, whose amplitudes then decrease until $t \approx$ 350–400 Ω_i^{-1}. Finally, the amplitudes of the transverse component stabilize after $t = 400\ \Omega_i^{-1}$. A critical divergence occurs in the behavior of the compressive component depending on the temperature of the beam ions. In Cases 1 and 2 with lower T_b, the compressive component saturates concurrently with the transverse component, and the ratio of compressive to total amplitude converges to approximately 0.2. In contrast, for Cases 3 and 4 with higher T_b, the compressive amplitude continues to grow. Notably, in Case 4, the compressive fluctuation eventually becomes the dominant component, with an amplitude ratio exceeding 0.5. This disparity suggests a fundamental difference introduced by the

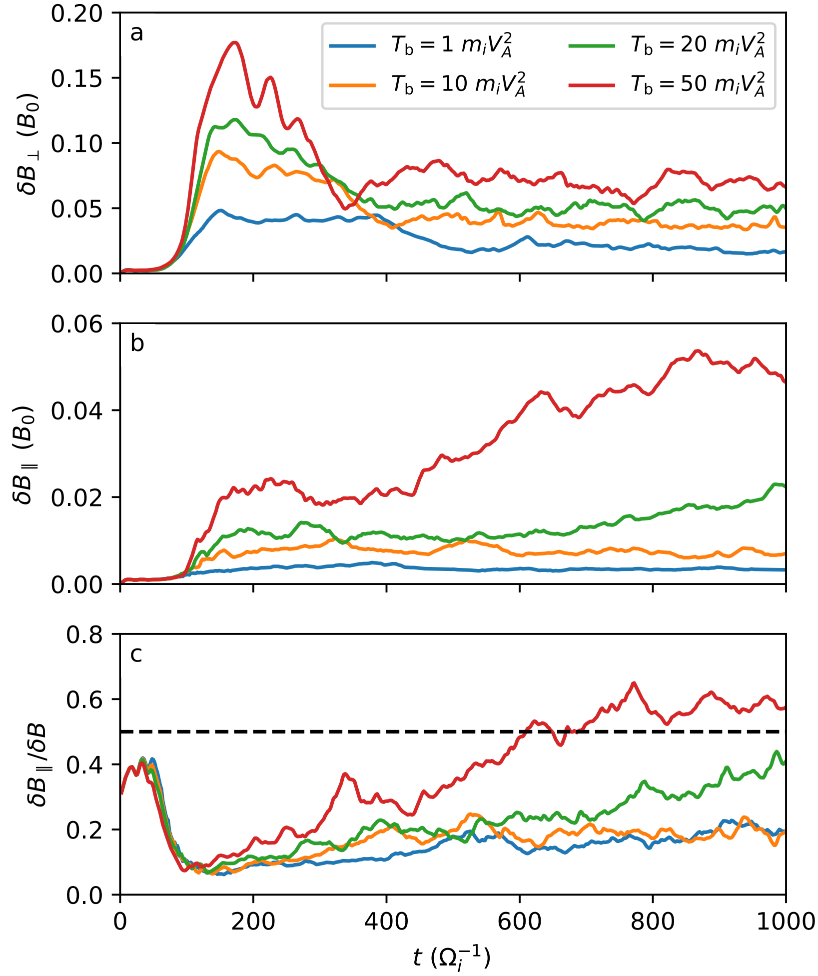

Figure 1. Temporal evolution of wave amplitudes: (a) transverse component $\delta B_\perp$, (b) compressive component $\delta B_\parallel$, and (c) the ratio of the compressive component to the total wave amplitude $\delta B_\parallel/\delta B$. The dashed line in panel (c) shows $\delta B_\parallel/\delta B = 0.5$, above which the compressive component takes dominance.

temperature of the beam ions. While the transverse component saturates similarly across all cases, the compressive modes require a sufficiently high temperature of the beam ions to sustain growth. We now examine the two extreme cases, Case 4 (Hot Beam) and Case 1 (Cool Beam), to investigate these processes in detail.

Figure 2 shows the spatial distribution of the magnetic field components (one of the transverse components δB_z, column a, and the compressive component δB_x, column b) and the dynamic pressure $P_d = m_i N_i V_i^2$ (column c) in Case 4, where the temperature of the beam ions is $T_b = 50\ m_i V_{A0}^2$. Parallel waves dominated by the transverse, circle-polarized fluctuation component are excited first via the right-hand instability as beam particles fill the simulation domain from the $-x$ boundary (Figure 2a1). Figure 3 plots the ion velocity distribution functions at the corresponding times. As shown in the figure, prior to $t = 100\ \Omega_i^{-1}$, these waves grow linearly, and the beam ions maintain a well-defined free-streaming Maxwellian distribution (Figures 3a1–3d1). These waves propagate in the $-x$ direction in the simulation frame, encountering denser, freshly injected beam ions.

As the wave amplitudes increase, significant scattering of beam ions occurs, generating a partial-shell ion distribution and scattering numerous ions back toward the $-x$ direction. This process depletes the free energy available for instability away from the injection boundary ($x = 0$), causing the amplitude of the parallel waves to decrease around $t = 200\ \Omega_i^{-1}$ (Figure 2a3). Simultaneously, nonlinear evolution disrupts the wave fronts, which

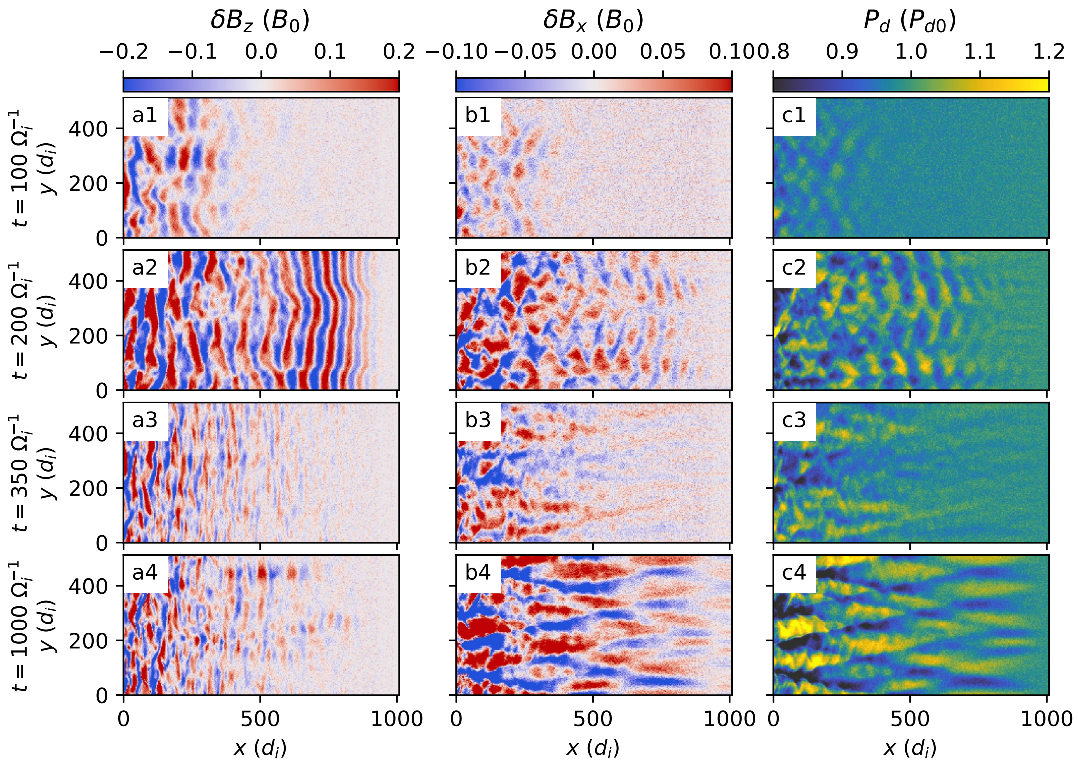

Figure 2. Spatial distribution of (a) fluctuations on magnetic field z-component δB_z, (b) fluctuations on magnetic field x-component δB_x, and (c) dynamic pressure P_d in Case 4 ($T_b = 50\ m_i V_{A0}^2$) at four distinct times.

become less coherent by $t = 350\ \Omega_i^{-1}$. Beyond this time, properties of the transverse component remain stable until the end of the simulation.

The compressive component evolves quite differently from the transverse component. Before $t = 200\ \Omega_i^{-1}$, compressive fluctuations correspond primarily to the x-component of the quasi-parallel propagating waves, with wave fronts oriented quasi-parallel to the y-direction. These fluctuations evolve synchronously with the transverse component. However, after $t \approx 350\ \Omega_i^{-1}$, distinct perpendicular modes with wave fronts parallel to the x-direction emerge. The amplitude of the perpendicular modes grows continuously, eventually becoming the dominant compressive fluctuation (Figure 2b4). Wave fronts belonging to these modes lie quasi-parallel to the x axis, while the propagating speed is close to zero. These fluctuations strongly modulate the plasma density and, consequently, the dynamic pressure. In the late stage of the simulation (Figure 2c4), the dynamic pressure exhibits ribbon-like structures resembling the compressive structures observed in the foreshock regions of hybrid simulations of collisionless shocks (Omidi, 2007; Ren et al., 2023), and the other physical properties of the structures in this simulation also agree with those of foreshock compressive structures.

Figure 4 shows the Fourier spectra of the transverse and compressive components for Case 4. For the transverse component, the initial waves peak around $k_x \simeq 0.08\ d_i^{-1}$ and $|k_y| < 0.04\ d_i^{-1}$ prior to $t = 200\ \Omega_i^{-1}$ (Figure 4a). Subsequently, the waves with larger parallel wave numbers are excited (Figures 4a2 and 4a3), corresponding to the slower beam particles arriving later in the $+x$ part of the simulation domain. This creates a spatial stratification where higher-energy beam ions are scattered first further into the background; consequently, the beam ion velocity distribution develops a two-layered partial shell structure around $t = 350\ \Omega_i^{-1}$ at $x \geq 450\ d_i$ (Figures 3b3–3d3). In the late stage of the simulation, the power of the transverse component is concentrated within $k_x \in (0.05, 0.15)\ d_i^{-1}$ (Figure 4a4).

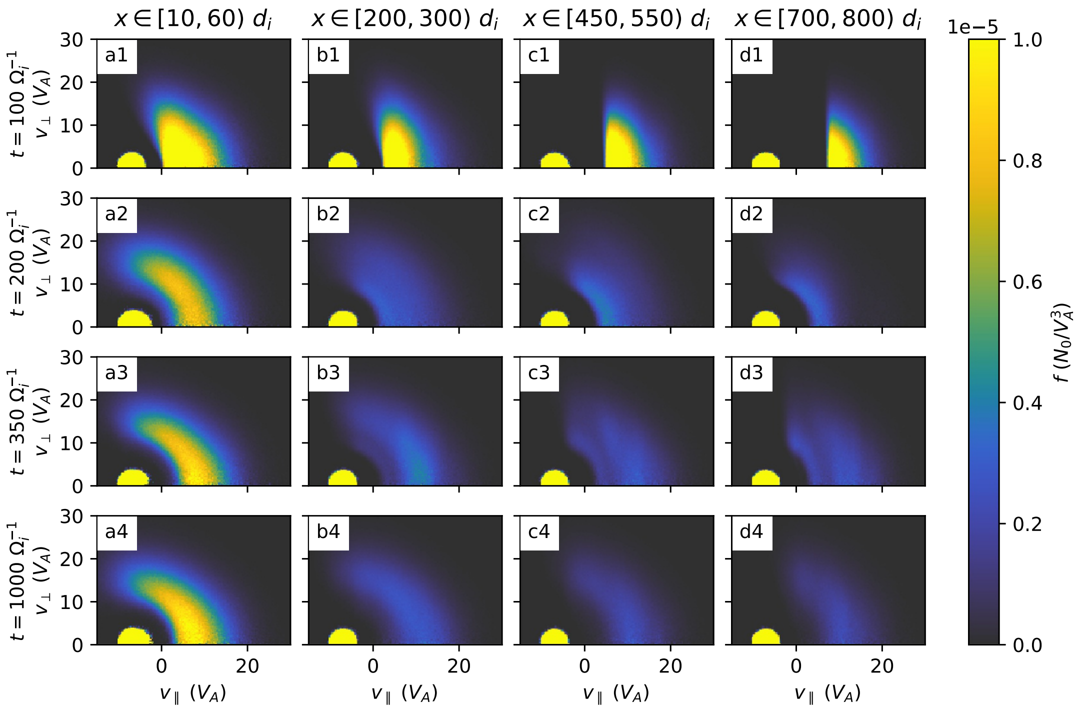

Figure 3. Ion velocity distribution function f in Case 4 ($T_b = 50\ m_i V_{A0}^2$). Distribution functions are sampled from ions within (a) $x \in [10, 60)\ d_i$, (b) $[200, 300)\ d_i$, (c) $[450, 500)\ d_i$, and (d) $[700, 800)\ d_i$.

The compressive component spectrum reveals two distinct types. The first occupies a spectral range similar to the transverse component, corresponding to the quasi-parallel propagating waves. The quasi-perpendicular modes with $k_x < 0.03$ and $|k_y| < 0.08$, emerge starting at $t \simeq 200\ \Omega_i^{-1}$ (Figure 4b2). Following the saturation of the quasi-parallel modes ($t > 350\ \Omega_i^{-1}$), the quasi-perpendicular modes gradually become dominant. The wave normal angle is approximately 80° relative to the x axis, with power distributed within $|k_y| < 0.1\ d_i^{-1}$, peaking at $k_y \simeq \pm\ 0.05\ d_i^{-1}$ (Figure 4b4).

We compare these results with Case 1, where the temperature of the beam ions is low ($T_b = 1\ m_i V_A^2$). Figure 5 shows the distribution of transverse and compressive components and the dynamic pressure. Similar to the hot beam case, quasi-parallel waves are excited first; however, these waves are more oblique with shorter wavelengths. As shown in Figure 6a1, the wave amplitude peaks near $k_x = 0.1\ d_i^{-1}$ and $k_y = \pm 0.05\ d_i^{-1}$, with power extending to perpendicular wave numbers of $k_y = \pm 0.15\ d_i^{-1}$. Saturation occurs when a sufficient number of particles are scattered by the waves. Concurrently, waves with shorter wavelength are excited by the scattered, slower beam ions, though their perpendicular wave number extent is narrower than that of the primary waves. In the late simulation stage, transverse fluctuation power concentrates in the perpendicular wave number domain while extending in the parallel domain ($k_x \in (0.1, 0.25)\ d_i^{-1}$, $|k_y| < 0.05\ d_i^{-1}$, Figures 6a3–6a4). At $t = 1000\ \Omega_i^{-1}$, there are small compressive structures formed near the $-x$ boundary. These structures may originate from the hot ions that are thermalized and trapped by the waves (Su et al., 2012), which in turn steepen the waves into shocklets or SLAMS (Schwartz & Burgess, 1991). Notably, the total saturation amplitude is approximately five times lower than in Case 4, and there are no obvious large-scale compressive structures observed during the simulation (Figures 5c1–5c4).

Due to the higher obliquity of the quasi-parallel waves in this case, the compressive fluctuations are initially dominated by these modes ($t < 200\ d_i^{-1}$). As the quasi-parallel waves saturate and their propagation vector becomes less oblique, the associated compressive power decreases. Unlike Case 4, the amplitude of the

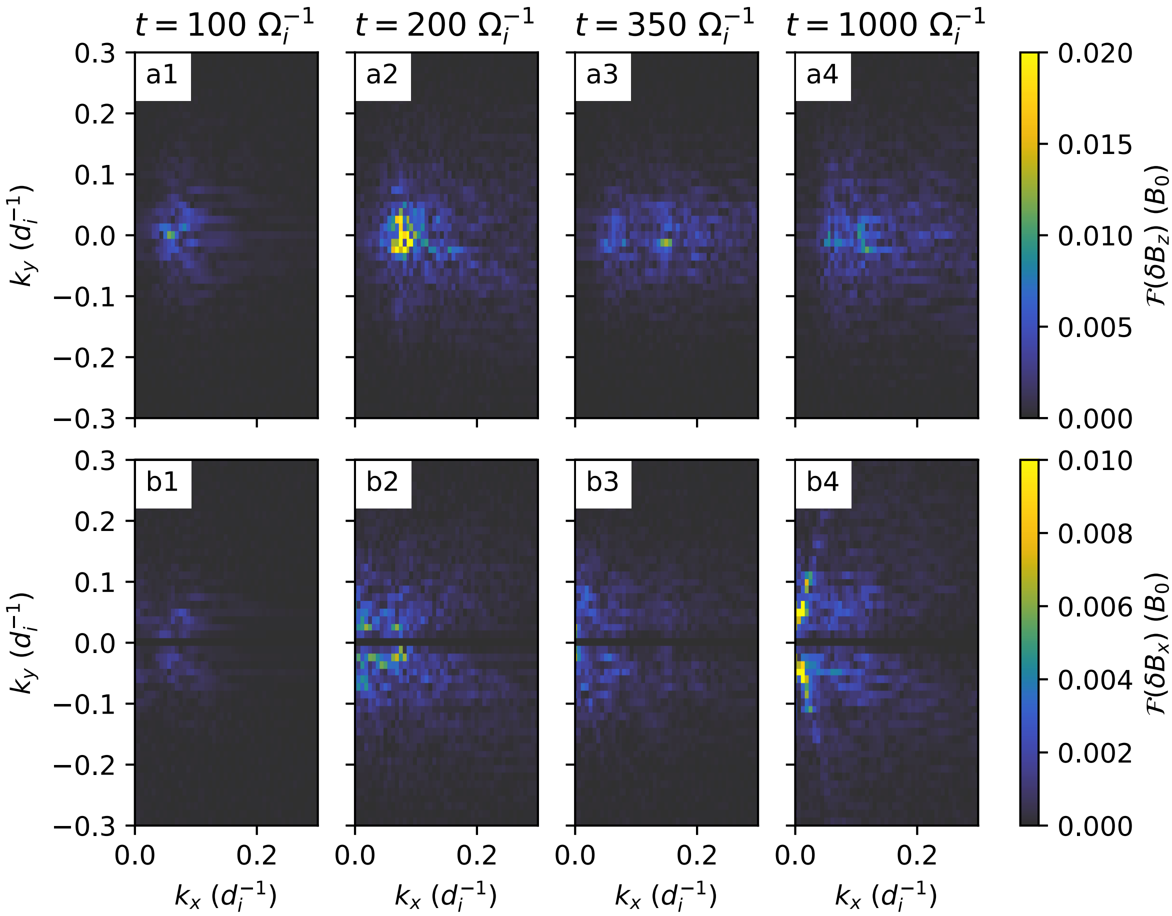

Figure 4. Fourier power spectra of the transverse (δB_z) and compressive (δB_x) wave components in Case 4 at different times.

perpendicular modes remains comparable to the noise levels throughout the simulation. The Fourier spectra in Figures 6b3–6b4 show only slight power increases within $k_x < 0.03\ d_i^{-1}$.

Figure 7 shows the ion velocity distribution for Case 1. The beam ions are significantly more concentrated than in Case 4 due to the lower temperature. Upon interaction with the waves, they scatter to form a partial-shell distribution (Figures 7a2–7d2). The sequential excitation of waves with varying wavenumbers leads to the formation of a two-layered partial-shell distribution in the later stages (Figures 7b3–7d4).

4. Conclusions and Discussion

This study investigates the formation of compressive structures associated with ion-ion beam instabilities using 2D hybrid simulations with continuously injected ion beams. Quasi-parallel propagating waves are excited first by the instabilities and saturate in amplitude during the subsequent wave-particle interactions. However, when the ion beam is sufficiently hot—a typical condition in the vicinity of a quasi-parallel shock front (Bonifazi & Moreno, 1981; Fuselier, 2013; Kempf et al., 2015)—perpendicular, nearly non-propagating wave modes can grow to a significant amplitude and form compressive structures, whereas these modes saturate at very low amplitudes when the temperature of the beam ions is low.

Compressive filamentary structures have been observed in prior hybrid simulations of ion-ion beam instabilities without continuous beam injection (Hellinger & Mangeney, 1999; Wang & Lin, 2006). These structures share significant similarities with the compressive structures presented in this work, including their non-propagating nature and the correlation between the magnetic field and plasma density. The primary difference is that these

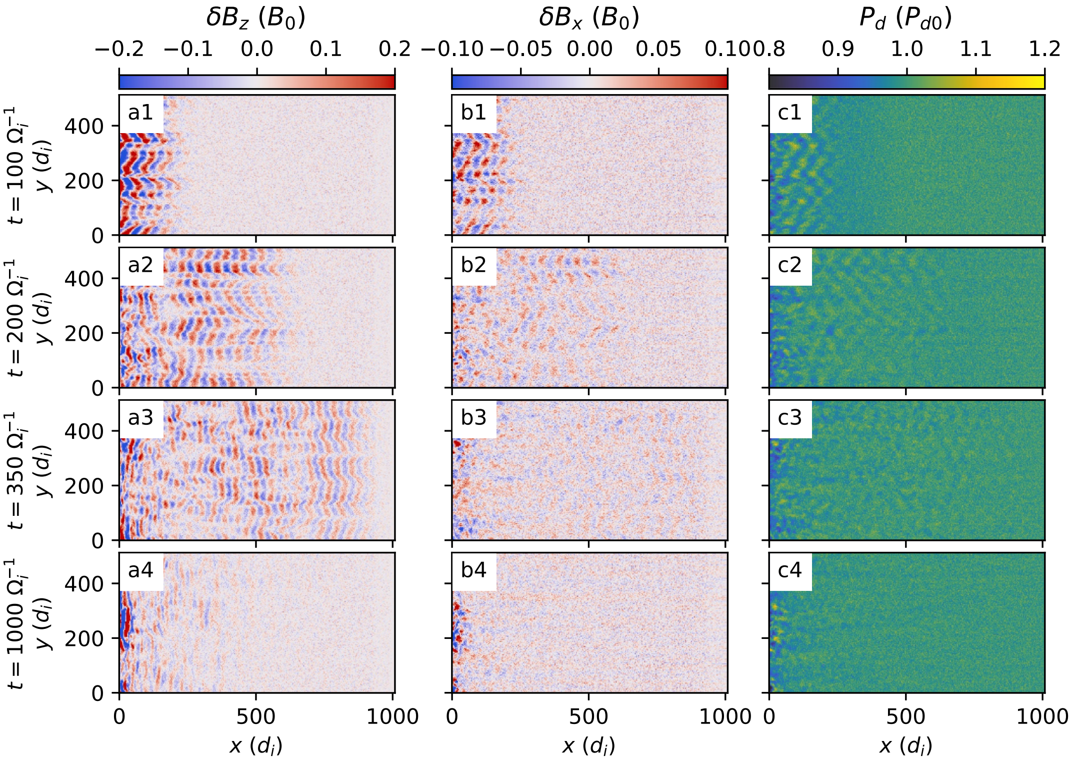

Figure 5. Spatial distribution of (a) fluctuations on magnetic field z-component δB_z, (b) fluctuations on magnetic field x-component δB_x, and (c) dynamic pressure P_d in Case 1 ($T_b = 1\ m_i V_{A0}^2$) at four distinct times.

previously reported filamentary structures exhibit much lower amplitudes and fade out during the late stages of the simulation (Hellinger & Mangeney, 1999). The setup of Case 4 in this study, which yields large-amplitude compressive structures, differs from the configurations used by Hellinger and Mangeney (1999) and Wang and Lin (2006) in two major aspects. First, the beam temperature is substantially higher in Case 4 (50 $m_i V_A^2$ vs. 0.25 $m_i V_A^2$ or 0.005 $m_i V_A^2$); second, the beam ions are continuously supplied throughout our simulations. To confirm that the beam temperature is not the sole decisive parameter governing the formation of these compressive structures, we conducted an additional simulation. This run utilized the same plasma parameters as Case 4 within an $n_x \times n_y = 512 \times 1008$ domain, employing periodic boundaries in the x-direction and omitting beam injection. As shown in Figure 8, the compressive δB_x component exhibits only non-coherent fluctuations at $t = 100\ \Omega_i^{-1}$, and its amplitude decreases over time during subsequent evolution. Therefore, the sustained supply of beam ions and a sufficiently high beam temperature are both indispensable conditions for the formation of large-amplitude compressive structures.

Quasi-perpendicular modes have been investigated in prior hybrid simulations of quasi-parallel shocks. Omidi (2007) observed these waves in a global hybrid simulation, naming them fast linearly polarized oblique waves based on their polarization properties. Subsequent work (Blanco-Cano et al., 2009) suggests that these waves are associated with field-aligned ion beams, specifically the ring-beam or diffused beam ions. Linear theory analysis based on a local hybrid simulation (Hao et al., 2021) demonstrates that shell-like distributed ions can contribute a positive growth rate to a quasi-perpendicular, compressive, and nearly non-propagating mode. This discrepancy may arise because the fitting function employed by the authors cannot accurately model the shell-like distribution (Hao et al., 2021), or it may indicate the involvement of a nonlinear mechanism.

The nonlinear superposition of two quasi-parallel waves with similar parallel wavevectors and frequencies can induce a second-order quasi-perpendicular perturbation in the magnetic pressure term, which subsequently evolves into pressure-balanced structures (Vasquez & Hollweg, 1999). In our simulations, the magnetic field

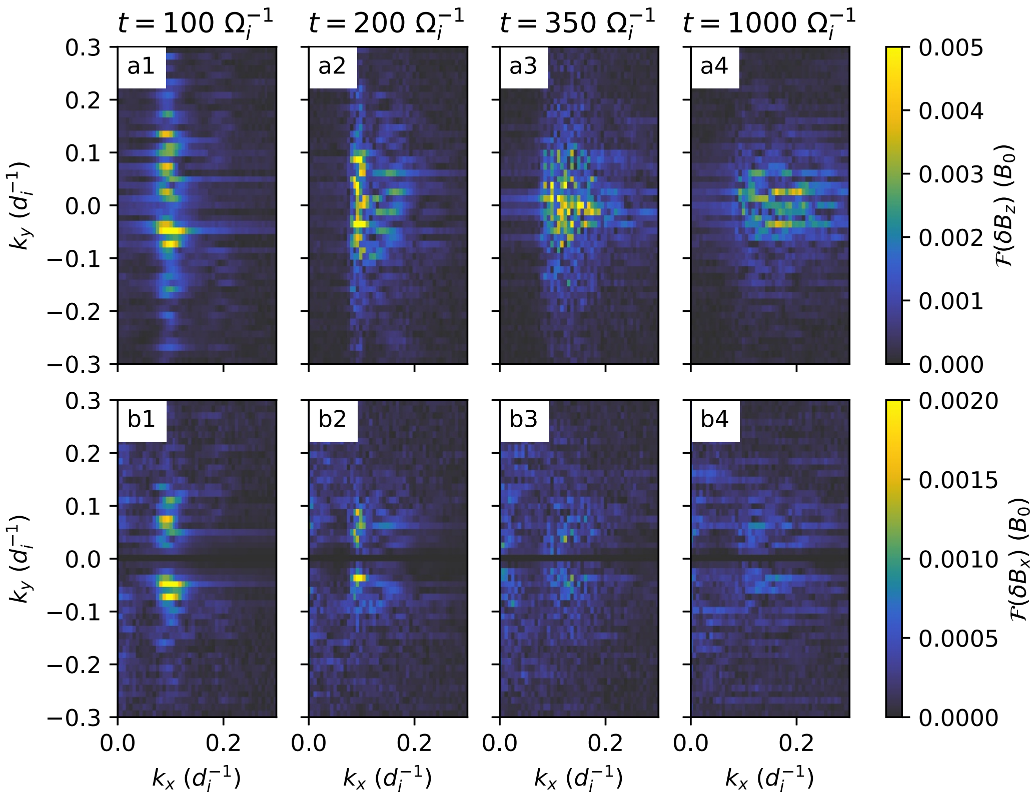

Figure 6. Fourier power spectra of the transverse (δB_z) and compressive (δB_x) wave components in Case 1 at different times. Note that the color limit is several times smaller than that of Figure 4 to keep the fluctuation visible.

strength is positively correlated and in-phase with the plasma density. Pressure balance is achieved through the thermal pressure of the beam ions (Figure 9), similar to the findings reported by Wang and Lin (2006) in simulations without continuous beam injection. Therefore, to maintain a stable, large-amplitude compressive structure, the beam ions must possess sufficient thermal energy to balance both the magnetic pressure and the thermal pressure of the background ions. This requirement likely explains why these structures are exclusively observed in simulations with a high beam temperature. Furthermore, to sustain the growth of the second-order fluctuations, the fundamental quasi-parallel waves must remain stable and continuously provide the necessary perturbation. In a system lacking sustained beam injection, the quasi-parallel waves are excited by the initial beam ions and rapidly exhaust their free energy. Although these waves can persist for a long period, the perpendicular perturbation they are able to provide remains limited. In our simulations, the quasi-parallel waves are continually excited by the continuously injected beam ions, thereby constantly amplifying the compressive structures to the maximum amplitude that the thermal energy of the beam ions can sustain.

The simulations in this study employ uniform beam injection from the boundary and high background species speeds to prevent shock formation within the simulation domain. The observation of compressive structures under these conditions implies that their formation is a primary foreshock process, independent of shock-front inhomogeneity (e.g., Hao et al., 2016). The conditions necessary for the formation of these structures, including sufficient beam temperatures and a sustained supply of beam ions, are commonly satisfied in the vicinity of quasi-parallel shocks. Consequently, magnetosheath jets generated by these compressive structures can be considered the result of the downstream convection of upstream inhomogeneities.

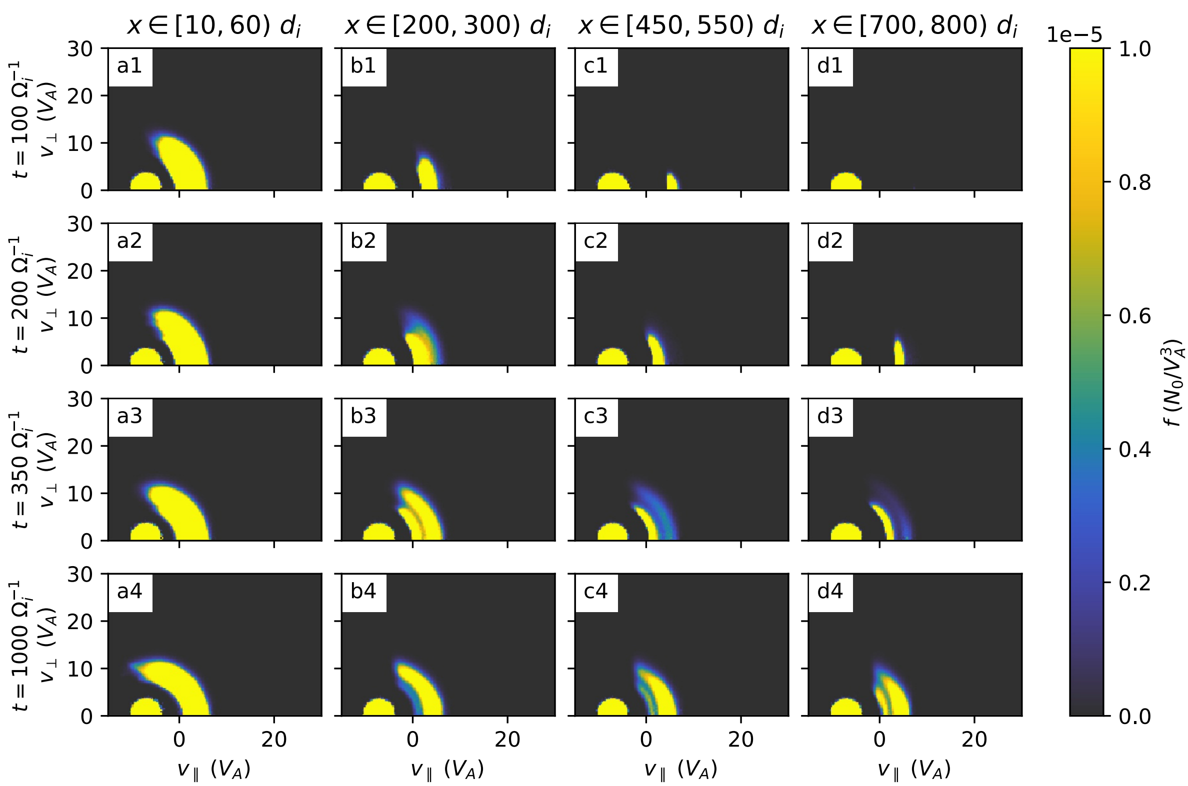

Figure 7. Ion velocity distribution function f in Case 1 ($T_b = 1\ m_i V_{A0}^2$). Distribution functions are sampled from ions within (a) $x \in [10, 60)\ d_i$, (b) $[200, 300)\ d_i$, (c) $[450, 550)\ d_i$, and (d) $[700, 800)\ d_i$.

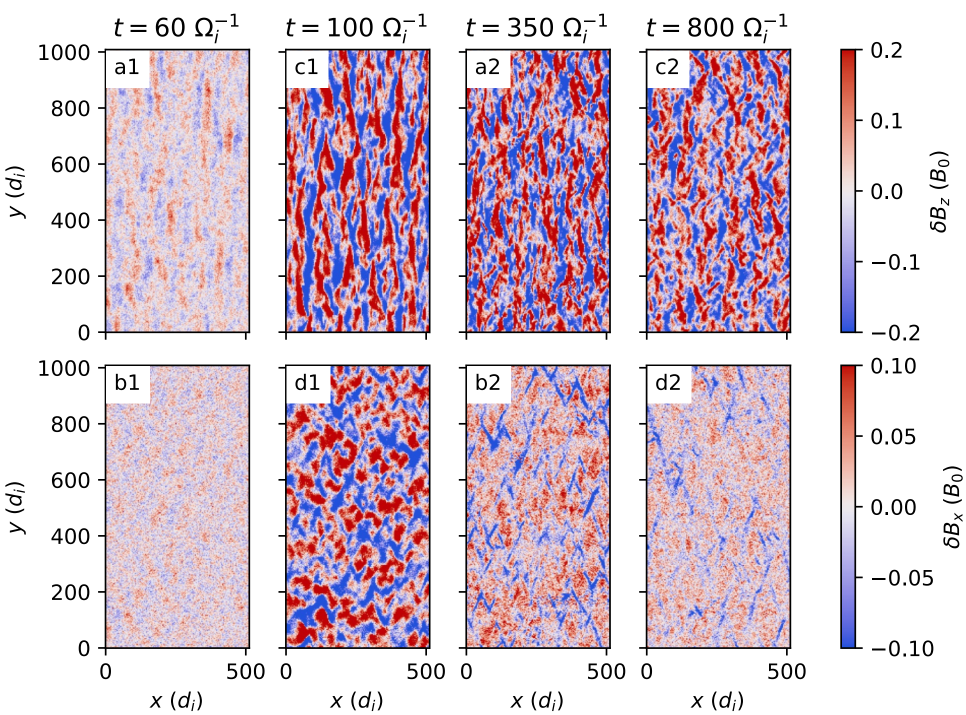

Figure 8. Spatial distribution of (a) fluctuations on magnetic field z-component δB_z and (b) fluctuations on magnetic field x-component δB_x. The plasma parameters are identical to Case 4, but the x boundaries of the simulation domain are periodic, and there are no plasma injections.

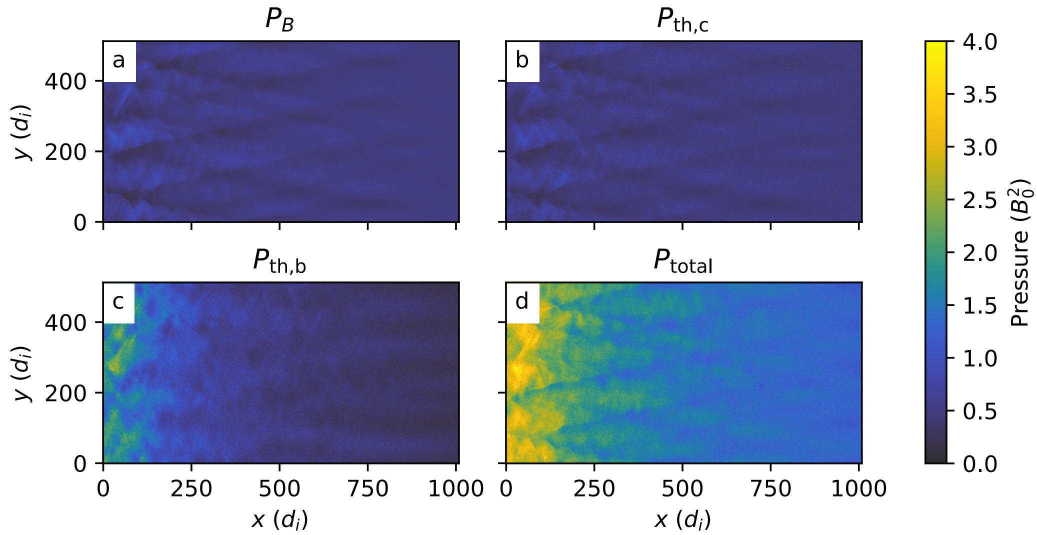

Figure 9. Magnetic pressure P_b (a), Thermal pressure of the background $P_{\mathrm{th,c}}$ (b) and beam ions $P_{\mathrm{th,b}}$ (c), and the total pressure $P_{\mathrm{total}} = P_b + P_{\mathrm{th,c}} + P_{\mathrm{th,b}}$.

Conflict of Interest

The authors declare no conflicts of interest relevant to this study.

Availability Statement

The simulation data and the specific version of the code used to produce the results in this paper (the `hybridVPIC` branch of the VPIC-Kokkos framework) are permanently archived and publicly accessible at the National Space Science Data Center, National Science and Technology Infrastructure of China (Ren, 2026). The original, open-source VPIC-Kokkos simulation framework is developed by third parties and is publicly available on GitHub at https://github.com/lanl/vpic-kokkos.

Acknowledgments
This research was funded by the National Key Research and Development Program of China (Grant. 2022YFA1604600), and the computer resources were provided by the Hefei Advanced Computing Center of China.

References

Archer, M. O., Hietala, H., Hartinger, M. D., Plaschke, F., & Angelopoulos, V. (2019). Direct observations of a surface eigenmode of the dayside magnetopause. *Nature Communications*, *10*(1), 615. https://doi.org/10.1038/s41467-018-08134-5

Archer, M. O., & Horbury, T. S. (2013). Magnetosheath dynamic pressure enhancements: Occurrence and typical properties. *Annales Geophysicae*, *31*(2), 319–331. https://doi.org/10.5194/angeo-31-319-2013

Archer, M. O., Horbury, T. S., & Eastwood, J. P. (2012). Magnetosheath pressure pulses: Generation downstream of the bow shock from solar wind discontinuities. *Journal of Geophysical Research: Space Physics*, *117*(A5). https://doi.org/10.1029/2011ja017468

Blanco-Cano, X., Omidi, N., & Russell, C. T. (2009). Global hybrid simulations: Foreshock waves and cavitons under radial interplanetary magnetic field geometry. *Journal of Geophysical Research: Space Physics*, *114*(A1). https://doi.org/10.1029/2008ja013406

Bonifazi, C., & Moreno, G. (1981). Reflected and diffuse ions backstreaming from the earth's bow shock 1. Basic properties. *Journal of Geophysical Research*, *86*(A6), 4397–4404. https://doi.org/10.1029/ja086ia06p04397

Burgess, D. (1989). Cyclic behavior at quasi-parallel collisionless shocks. *Geophysical Research Letters*, *16*(5), 345–348. https://doi.org/10.1029/gl016i005p00345

Burgess, D., & Scholer, M. (2015). *Collisionless shocks in space plasmas: Structure and accelerated particles*. Cambridge University Press. Retrieved from. https://doi.org/10.1017/cbo9781139044097

Dmitriev, A. V., & Suvorova, A. V. (2012). Traveling magnetopause distortion related to a large-scale magnetosheath plasma jet: Themis and ground-based observations. *Journal of Geophysical Research: Space Physics*, *117*(A8). https://doi.org/10.1029/2011ja016861

Dubouloz, N., & Scholer, M. (1995). 2d hybrid simulations of short large-amplitude magnetic structures (slams) upstream of quasi-parallel collisionless shocks. *Advances in Space Research*, *15*(8–9), 175–178. https://doi.org/10.1016/0273-1177(94)00100-f

Eastwood, J. P., Balogh, A., Lucek, E. A., Mazelle, C., & Dandouras, I. (2003). On the existence of alfvén waves in the terrestrial foreshock. *Annales Geophysicae*, *21*(7), 1457–1465. https://doi.org/10.5194/angeo-21-1457-2003

Fairfield, D. H. (1969). Bow shock associated waves observed in the far upstream interplanetary medium. *Journal of Geophysical Research*, *74*(14), 3541–3553. https://doi.org/10.1029/ja074i014p03541

Fatemi, S., Hamrin, M., Krämer, E., Gunell, H., Nordin, G., Karlsson, T., & Goncharov, O. (2024). Unveiling the 3d structure of magnetosheath jets. *Monthly Notices of the Royal Astronomical Society*, *531*(4), 4692–4713. https://doi.org/10.1093/mnras/stae1456

Fuselier, S. A. (2013). Suprathermal ions upstream and downstream from the earth's bow shock. In *Solar wind sources of magnetospheric ultra-low-frequency waves* (pp. 107–119). American Geophysical Union. https://doi.org/10.1029/gm081p0107

Gary, S. (1991). Electromagnetic ion/ion instabilities and their consequences in space plasmas: A review. *Space Science Reviews*, *56*(3–4). https://doi.org/10.1007/bf00196632

Gary, S. P. (1978). The electromagnetic ion beam instability and energy loss of fast alpha particles. *Nuclear Fusion*, *18*(3), 327–334. https://doi.org/10.1088/0029-5515/18/3/003

Gary, S. P. (1985). Electromagnetic ion beam instabilities - Hot beams at interplanetary shocks. *The Astrophysical Journal*, *288*, 342. https://doi.org/10.1086/162797

Gingell, I., Schwartz, S. J., Burgess, D., Johlander, A., Russell, C. T., Burch, J. L., et al. (2017). Mms observations and hybrid simulations of surface ripples at a marginally quasi-parallel shock. *Journal of Geophysical Research: Space Physics*, *122*(11). https://doi.org/10.1002/2017ja024538

Gosling, J. T., Thomsen, M. F., Bame, S. J., & Russell, C. T. (1989). Ion reflection and downstream thermalization at the quasi-parallel bow shock. *Journal of Geophysical Research*, *94*(A8), 10027–10037. https://doi.org/10.1029/ja094ia08p10027

Gunell, H., Hamrin, M., Nesbit-Östman, S., Krämer, E., & Nilsson, H. (2023). Magnetosheath jets at mars. *Science Advances*, *9*(22), eadg5703. https://doi.org/10.1126/sciadv.adg5703

Guo, J., Lu, S., Lu, Q., Lin, Y., Wang, X., Ren, J., et al. (2022). Large-scale high-speed jets in earth's magnetosheath: Global hybrid simulations. *Journal of Geophysical Research: Space Physics*, *127*(6), e2022JA030477. https://doi.org/10.1029/2022ja030477

Guo, J., Lu, S., Lu, Q., Ren, J., Ma, J., Slavin, J. A., et al. (2024). Three-dimensional global hybrid simulation of magnetosheath jets at mercury. *The Astrophysical Journal Letters*, *978*(1), L9. https://doi.org/10.3847/2041-8213/ad9dd7

Guo, J., Lu, S., Lu, Q., Wang, B., Wang, S., Ren, J., et al. (2026). Large-scale distortion of the dayside magnetopause under radial interplanetary magnetic field. *Science Bulletin*. https://doi.org/10.1016/j.scib.2026.01.032

Han, D., Nishimura, Y., Lyons, L. R., Hu, H., & Yang, H. (2016). Throat aurora: The ionospheric signature of magnetosheath particles penetrating into the magnetosphere. *Geophysical Research Letters*, *43*(5), 1819–1827. https://doi.org/10.1002/2016gl068181

Hao, Y., Gao, X., Lu, Q., Huang, C., Wang, R., & Wang, S. (2017). Reformation of rippled quasi-parallel shocks: 2-d hybrid simulations. *Journal of Geophysical Research: Space Physics*, *122*(6), 6385–6396. https://doi.org/10.1002/2017ja024234

Hao, Y., Lu, Q., Gao, X., & Wang, S. (2016). Ion dynamics at a rippled quasi-parallel shock: 2d hybrid simulations. *The Astrophysical Journal*, *823*(1), 7. https://doi.org/10.3847/0004-637x/823/1/7

Hao, Y., Lu, Q., Wu, D., Lu, S., Xiang, L., & Ke, Y. (2021). Low-frequency waves upstream of quasi-parallel shocks: Two-dimensional hybrid simulations. *The Astrophysical Journal*, *915*(1), 64. https://doi.org/10.3847/1538-4357/ac02ce

Hellinger, P., & Mangeney, A. (1999). Electromagnetic ion beam instabilities: Oblique pulsations. *Journal of Geophysical Research*, *104*(A3), 4669–4680. https://doi.org/10.1029/1998JA900157

Hietala, H., Laitinen, T. V., Andréeová, K., Vainio, R., Vaivads, A., Palmroth, M., et al. (2009). Supermagnetosonic jets behind a collisionless quasiparallel shock. *Physical Review Letters*, *103*(24), 245001. https://doi.org/10.1103/physrevlett.103.245001

Hietala, H., Trotta, D., Fedeli, A., Wilson, L. B., Vuorinen, L., & Coburn, J. T. (2024). Candidates for downstream jets at interplanetary shocks. *Monthly Notices of the Royal Astronomical Society*, *531*(2), 2415–2421. https://doi.org/10.1093/mnras/stae1294

Hoppe, M. M., & Russell, C. T. (1983). Plasma rest frame frequencies and polarizations of the low-frequency upstream waves: Isee 1 and 2 observations. *Journal of Geophysical Research*, *88*(A3), 2021–2027. https://doi.org/10.1029/ja088ia03p02021

Karlsson, T., Liljeblad, E., Kullen, A., Raines, J. M., Slavin, J. A., & Sundberg, T. (2016). Isolated magnetic field structures in mercury's magnetosheath as possible analogues for terrestrial magnetosheath plasmoids and jets. *Planetary and Space Science*, *129*, 61–73. https://doi.org/10.1016/j.pss.2016.06.002

Kempf, Y., Pokhotelov, D., Gutynska, O., Wilson III, L. B., Walsh, B. M., Alfthan, S. v., et al. (2015). Ion distributions in the earth's foreshock: Hybrid-vlasov simulation and themis observations. *Journal of Geophysical Research: Space Physics*, *120*(5), 3684–3701. https://doi.org/10.1002/2014ja020519

Le, A., Stanier, A., Yin, L., Wetherton, B., Keenan, B., & Albright, B. (2023). Hybrid-vpic: An open-source kinetic/fluid hybrid particle-in-cell code. *Physics of Plasmas*, *30*(6), 063902. https://doi.org/10.1063/5.0146529

Leroy, M. M., Winske, D., Goodrich, C. C., Wu, C. S., & Papadopoulos, K. (1982). The structure of perpendicular bow shocks. *Journal of Geophysical Research*, *87*(A7), 5081–5094. https://doi.org/10.1029/ja087ia07p05081

Lin, Y., Lee, L. C., & Yan, M. (1996). Generation of dynamic pressure pulses downstream of the bow shock by variations in the interplanetary magnetic field orientation. *Journal of Geophysical Research*, *101*(A1), 479–493. https://doi.org/10.1029/95ja02985

Lu, Q. M., Xia, L. D., & Wang, S. (2006). Hybrid simulations of parallel and oblique electromagnetic alpha/proton instabilities in the solar wind. *Journal of Geophysical Research: Space Physics*, *111*(A9). https://doi.org/10.1029/2006ja011752

Ma, J., Tang, B., Gao, X., Li, W., Lu, Q., Guo, W., et al. (2024). The comprehensive response of the magnetopause to the impact of an isolated magnetosheath high-speed jet. *Geophysical Research Letters*, *51*(21), e2024GL111132. https://doi.org/10.1029/2024gl111132

Narita, Y., Glassmeier, K., Fornaçon, K., Richter, I., Schäfer, S., Motschmann, U., et al. (2006). Low-frequency wave characteristics in the upstream and downstream regime of the terrestrial bow shock. *Journal of Geophysical Research: Space Physics*, *111*(A1). https://doi.org/10.1029/2005ja011231

Němeček, Z., Šafránková, J., Grygorov, K., Mokrý, A., Pi, G., Aghabozorgi Nafchi, M., et al. (2023). Extremely distant magnetopause locations caused by magnetosheath jets. *Geophysical Research Letters*, *50*(24), e2023GL106131. https://doi.org/10.1029/2023gl106131

Němeček, Z., Šafránková, J., Přech, L., Sibeck, D. G., Kokubun, S., & Mukai, T. (1998). Transient flux enhancements in the magnetosheath. *Geophysical Research Letters*, *25*(8), 1273–1276. https://doi.org/10.1029/98gl50873

Omidi, N. (2007). Formation of cavities in the foreshock. *Aip conference proceedings*. (Vol. 932, pp. 181–190). AIP. https://doi.org/10.1063/1.2778962

Omidi, N., Zhang, H., Sibeck, D., & Turner, D. (2013). Spontaneous hot flow anomalies at quasi-parallel shocks: 2. hybrid simulations. *Journal of Geophysical Research: Space Physics*, *118*(1), 173–180. https://doi.org/10.1029/2012ja018099

Palmroth, M., Hietala, H., Plaschke, F., Archer, M., Karlsson, T., Blanco-Cano, X., et al. (2018). Magnetosheath jet properties and evolution as determined by a global hybrid-vlasov simulation. *Annales Geophysicae*, *36*(5), 1171–1182. https://doi.org/10.5194/angeo-36-1171-2018

Plaschke, F., Hietala, H., & Angelopoulos, V. (2013). Anti-sunward high-speed jets in the subsolar magnetosheath. *Annales Geophysicae*, *31*(10), 1877–1889. https://doi.org/10.5194/angeo-31-1877-2013

Plaschke, F., Hietala, H., Angelopoulos, V., & Nakamura, R. (2016). Geoeffective jets impacting the magnetopause are very common. *Journal of Geophysical Research: Space Physics*, *121*(4), 3240–3253. https://doi.org/10.1002/2016ja022534

Raptis, S., Karlsson, T., Vaivads, A., Lindberg, M., Johlander, A., & Trollvik, H. (2022). On magnetosheath jet kinetic structure and plasma properties. *Geophysical Research Letters*, *49*(21), e2022GL100678. https://doi.org/10.1029/2022gl100678

Ren, J. (2026). Data for "two-dimensional hybrid simulations of compressive structures formed during ion-ion beam instabilities" [Dataset]. *Science Data Bank*. https://doi.org/10.57760/sciencedb.34772

Ren, J., Guo, J., Lu, Q., Lu, S., Gao, X., Ma, J., & Wang, R. (2024). Honeycomb-like magnetosheath structure formed by jets: Three-dimensional global hybrid simulations. *Geophysical Research Letters*, *51*(12), e2024GL109925. https://doi.org/10.1029/2024gl109925

Ren, J., Lu, Q., Guo, J., Gao, X., Lu, S., Wang, S., & Wang, R. (2023). Two-dimensional hybrid simulations of high-speed jets downstream of quasi-parallel shocks. *Journal of Geophysical Research: Space Physics*, *128*(8), e2023JA031699. https://doi.org/10.1029/2023ja031699

Scholer, M., Fujimoto, M., & Kucharek, H. (1993). Two-dimensional simulations of supercritical quasi-parallel shocks: Upstream waves, downstream waves, and shock re-formation. *Journal of Geophysical Research*, *98*(A11), 18971–18984. https://doi.org/10.1029/93ja01647

Scholer, M., Kucharek, H., & Shinohara, I. (2003). Short large-amplitude magnetic structures and whistler wave precursors in a full-particle quasi-parallel shock simulation. *Journal of Geophysical Research: Space Physics*, *108*(A7). https://doi.org/10.1029/2002ja009820

Schwartz, S. J., & Burgess, D. (1991). Quasi-parallel shocks: A patchwork of three-dimensional structures. *Geophysical Research Letters*, *18*(3), 373–376. https://doi.org/10.1029/91gl00138

Su, Y., Lu, Q., Huang, C., Wu, M., Gao, X., & Wang, S. (2012). Particle acceleration and generation of diffuse superthermal ions at a quasi-parallel collisionless shock: Hybrid simulations. *Journal of Geophysical Research: Space Physics*, *117*(A8). https://doi.org/10.1029/2012ja017736

Suni, J., Palmroth, M., Turc, L., Battarbee, M., Johlander, A., Tarvus, V., et al. (2021). Connection between foreshock structures and the generation of magnetosheath jets: Vlasiator results. *Geophysical Research Letters*, *48*(20), e2021GL095655. https://doi.org/10.1029/2021gl095655

Tang, H.-b., Hao, Y.-f., Hu, G.-y., Lu, Q.-m., Ren, C., Zhang, Y., et al. (2025). Laboratory observation of ion drift acceleration via reflection off laser-produced magnetized collisionless shocks. *Science Advances*, *11*(7), eadn3320. https://doi.org/10.1126/sciadv.adn3320

Tsubouchi, K., & Lembège, B. (2004). Full particle simulations of short large-amplitude magnetic structures (slams) in quasi-parallel shocks. *Journal of Geophysical Research: Space Physics*, *109*(A2). https://doi.org/10.1029/2003ja010014

Vasquez, B. J., & Hollweg, J. V. (1999). Formation of pressure-balanced structures and fast waves from nonlinear alfvén waves. *Journal of Geophysical Research*, *104*(A3), 4681–4696. https://doi.org/10.1029/1998ja900090

Wang, B., Nishimura, Y., Hietala, H., Lyons, L., Angelopoulos, V., Plaschke, F., et al. (2018). Impacts of magnetosheath high-speed jets on the magnetosphere and ionosphere measured by optical imaging and satellite observations. *Journal of Geophysical Research: Space Physics*, *123*(6), 4879–4894. https://doi.org/10.1029/2017ja024954

Wang, X. Y., & Lin, Y. (2003). Generation of nonlinear alfvén and magnetosonic waves by beam–plasma interaction. *Physics of Plasmas*, *10*(9), 3528–3538. https://doi.org/10.1063/1.1599359

Wang, X. Y., & Lin, Y. (2006). Generation of filamentary structures by beam-plasma interaction. *Physics of Plasmas*, *13*(5), 052102. https://doi.org/10.1063/1.2197797

Yang, Z., Jarvinen, R., Guo, X., Sun, T., Koutroumpa, D., K. Parks, G., et al. (2024). Deformations at earth's dayside magnetopause during quasi-radial imf conditions: Global kinetic simulations and soft x-ray imaging. *Earth and Planetary Physics*, *8*(1), 59–69. https://doi.org/10.26464/epp2023059

Zhou, Y., Raptis, S., Wang, S., Shen, C., Ren, N., & Ma, L. (2024). Magnetosheath jets at jupiter and across the solar system. *Nature Communications*, *15*(1), 4. https://doi.org/10.1038/s41467-023-43942-4